Electronic Supplementary Material (ESI) for Journal of Materials Chemistry C.
This journal is © The Royal Society of Chemistry 2020

Supplementary Information

A light trigged optical and chiroptical switch based on a Eu_2L_3 Helicate

Jianpeng Zhang, Yanyan Zhou, Yuan Yao, Zhenyu Cheng, Ting Gao, Hongfeng Li* and Pengfei Yan

Key Laboratory of Functional Inorganic Material Chemistry, Ministry of Education, P. R. China; School of Chemistry and Materials Science, Heilongjiang University, Harbin 150080, P. R. China.

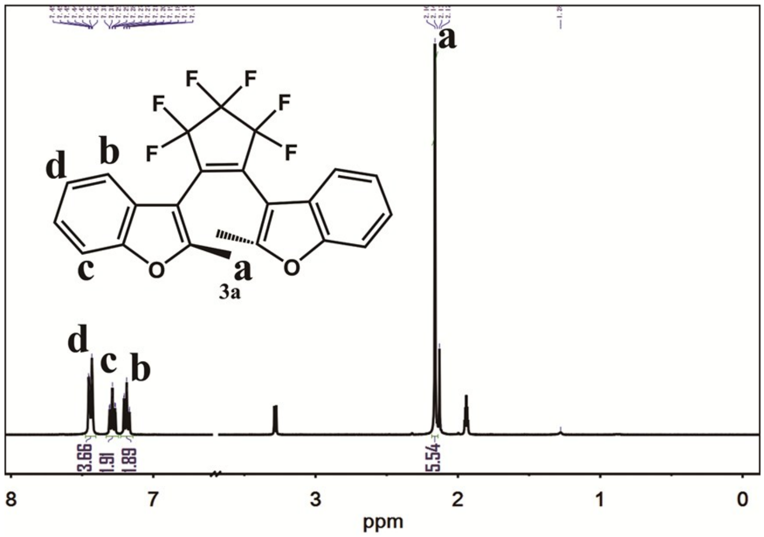

Figure S1. ^1H NMR spectrum of **3a** in CD_3CN.

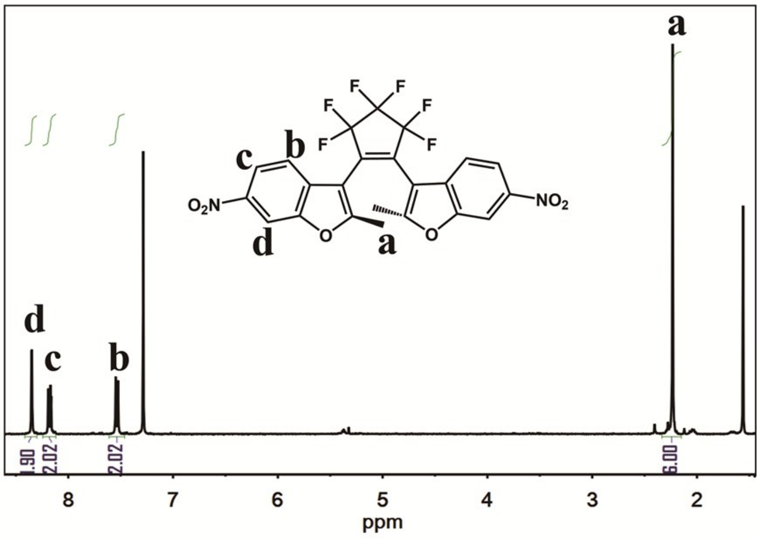

Figure S2. ^1H NMR spectrum of **4a** in $CDCl_3$

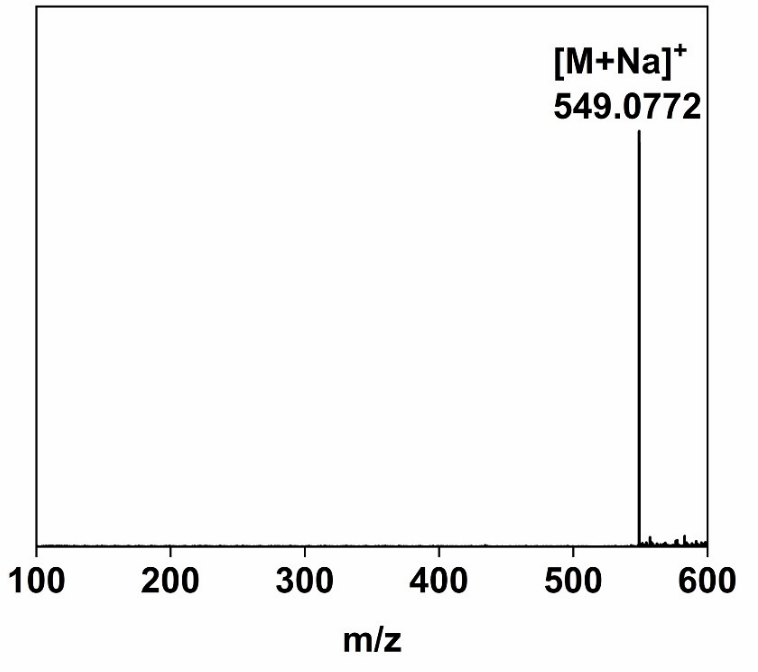

Figure S3. ESI-TOF-MS spectrum of **4a**.

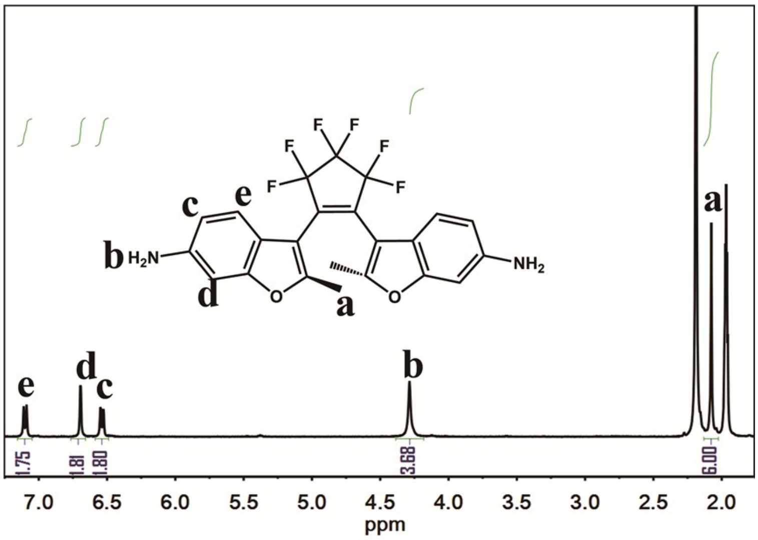

Figure S4. ^{1}H NMR spectrum of **5a** in CD_3CN.

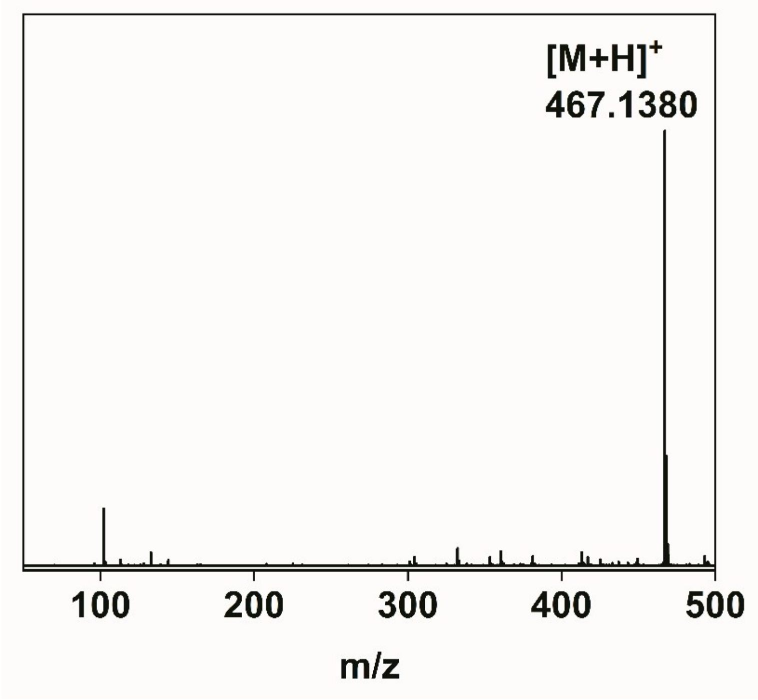

Figure S5. ESI-TOF-MS spectrum of **5a**.

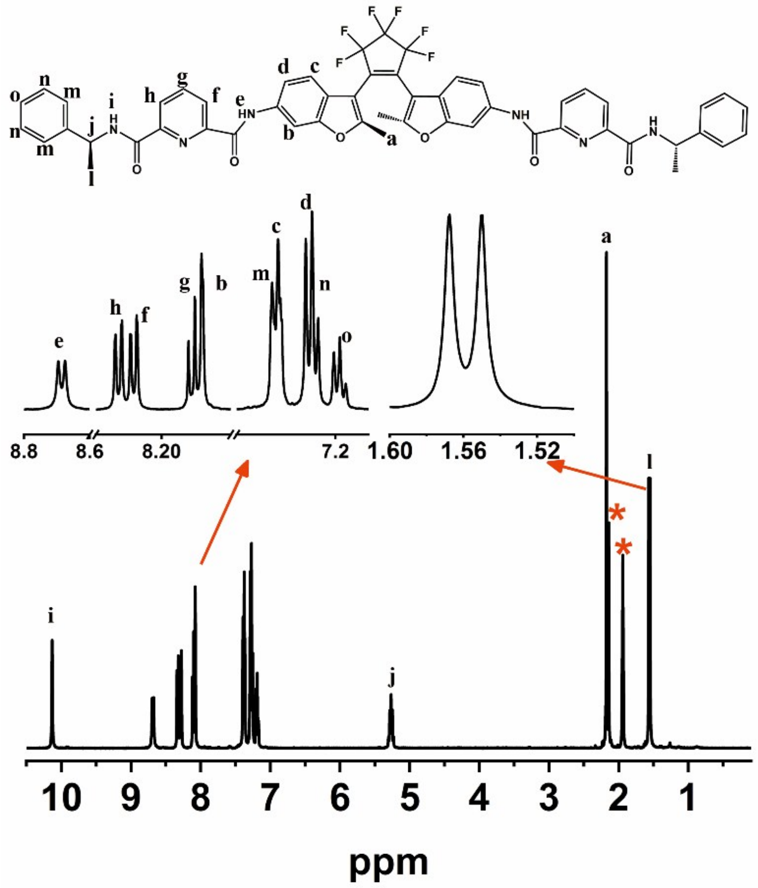

Figure S6. ^{1}H NMR spectrum of o-**L**^{RR} in CD_3CN.

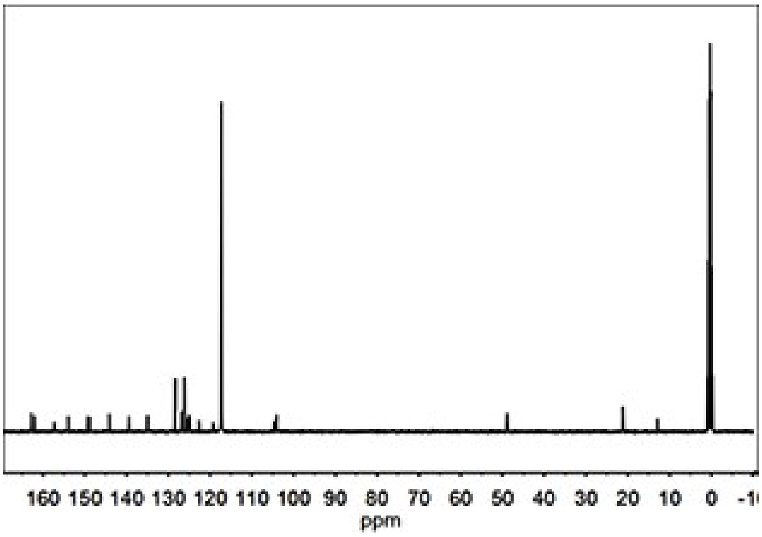

Figure S7. ^{13}C NMR spectrum of o-$\mathbf{L}^{RR}$ in CD_3CN.

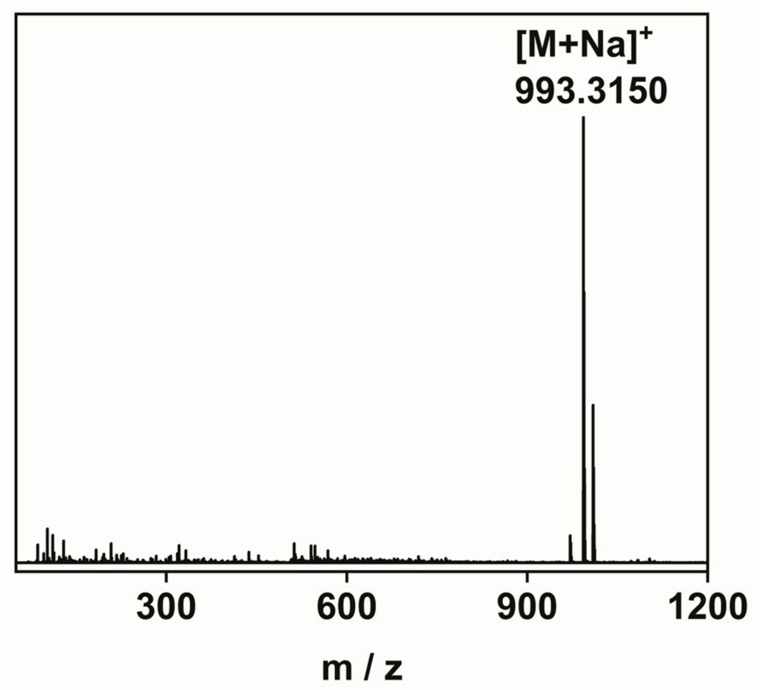

Figure S8. ESI-TOF-MS spectrum of o-$\mathbf{L}^{RR}$.

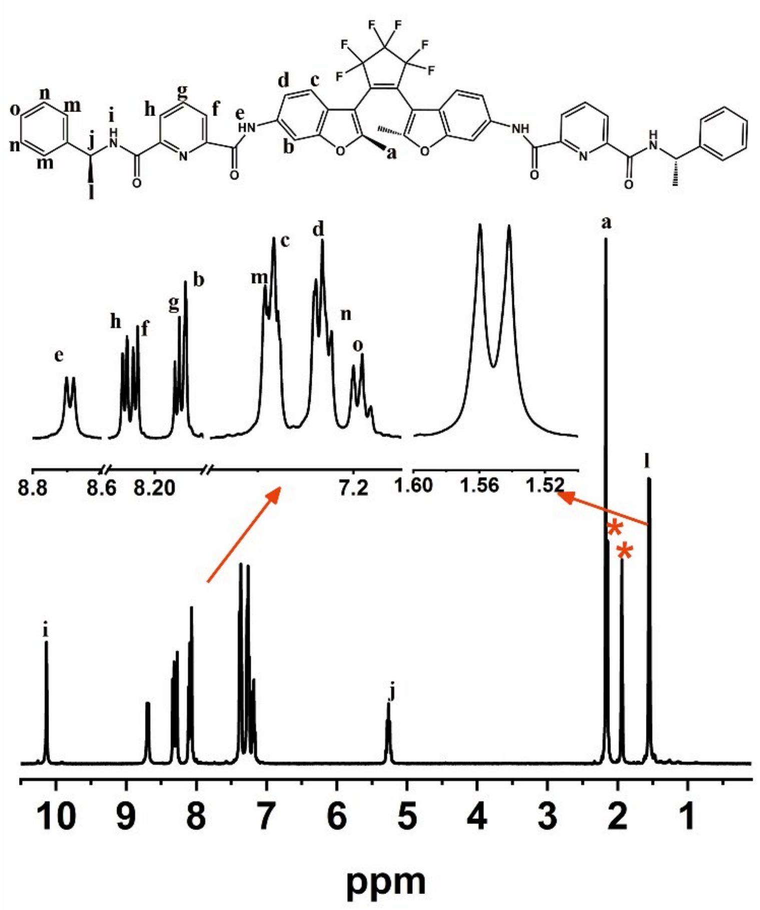

Figure S9. ^{1}H NMR spectrum of o-**L**^{SS} in CD_3CN.

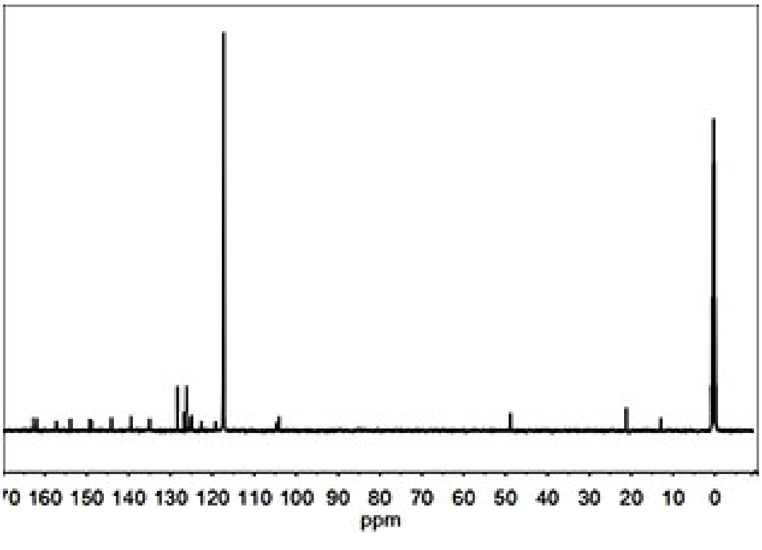

Figure S10. ^{13}C NMR spectrum of o-**L**^{SS} in CD_3CN.

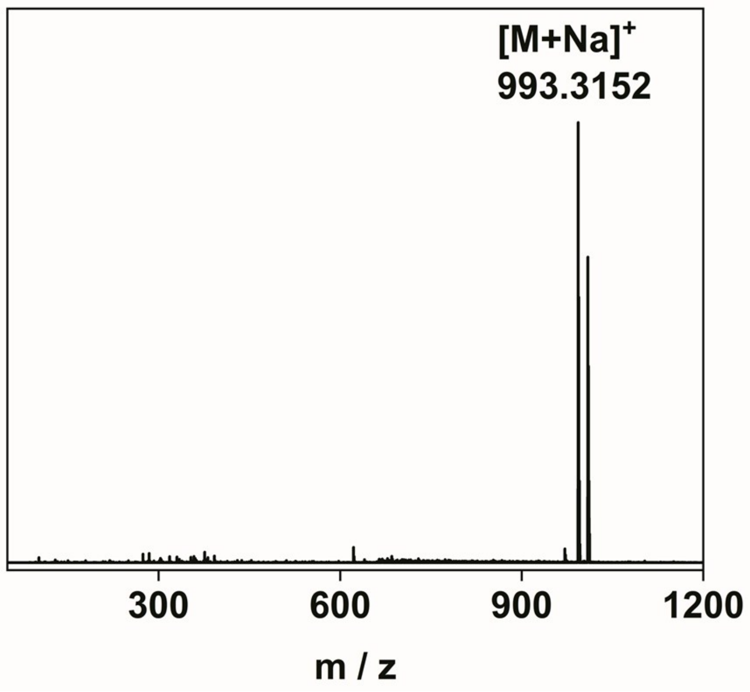

Figure S11. ESI-TOF-MS spectrum of o-**L**^{SS}

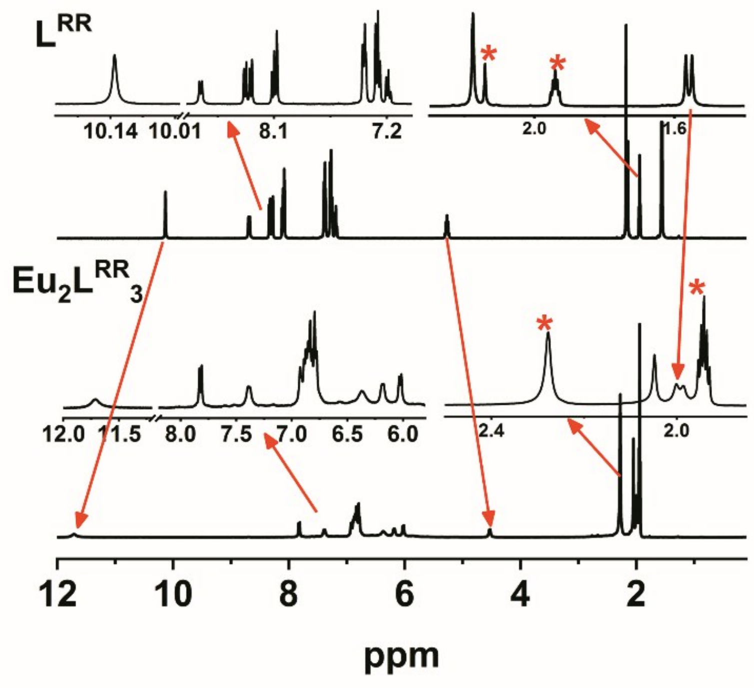

Figure S12. ^{1}H NMR spectra of o-**L**^{RR} and [Eu$_2$(o-**L**^{RR})$_3$](TOf)$_6$ in CD$_3$CN.

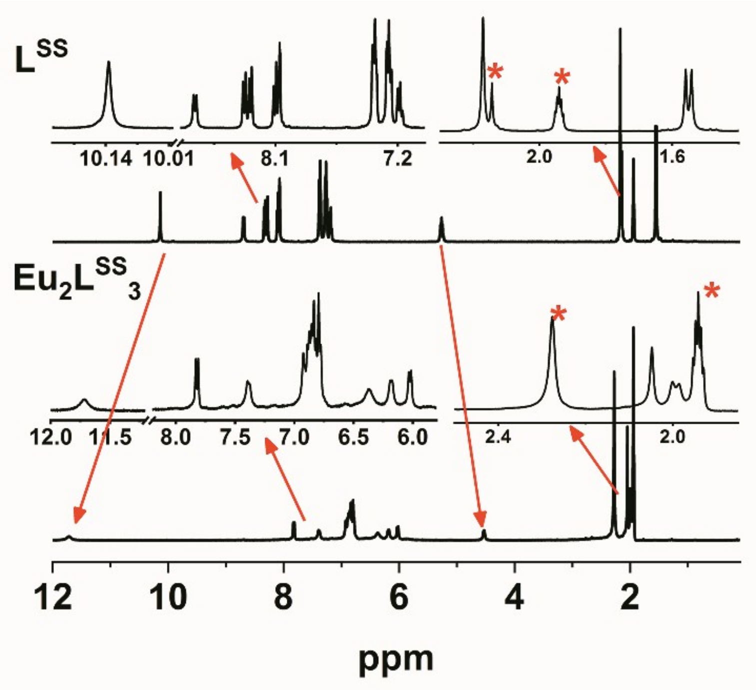

Figure S13. ^{1}H NMR spectra of o-$\mathbf{L}^{SS}$ and [Eu_2(o-$\mathbf{L}^{SS}$)$_3$](TOf)$_6$ in CD_3CN.

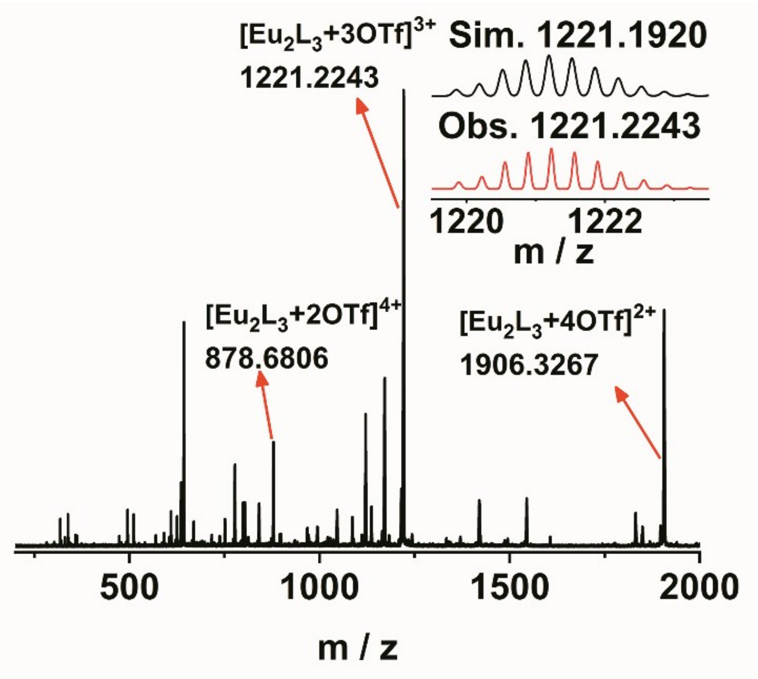

Figure S14. ESI-TOF-MS spectrum of helicate [(Eu_2 (o-$\mathbf{L}^{SS}$)$_3$](TOf)$_6$ with insets showing the observed (Obs.) and simulated (Sim.) isotopic patterns of the anion [[Eu_2 (o-$\mathbf{L}^{SS}$)$_3$](TOf)$_3$]$^{3+}$ peaks.

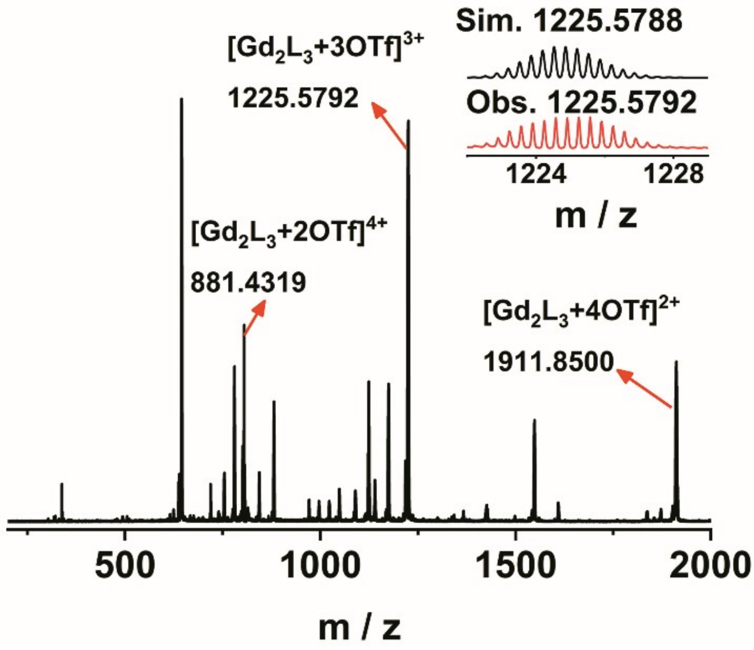

Figure S15. ESI-TOF-MS spectrum of helicate $[\mathrm{Gd_2}(\mathrm{o}\text{-}\mathbf{L}^{RR})_3](\mathrm{TOf})_6$ with insets showing the observed (Obs.) and simulated (Sim.) isotopic patterns of the anion $[[\mathrm{Gd_2}(\mathrm{o}\text{-}\mathbf{L}^{RR})_3](\mathrm{TOf})_3]^{3+}$ peaks.

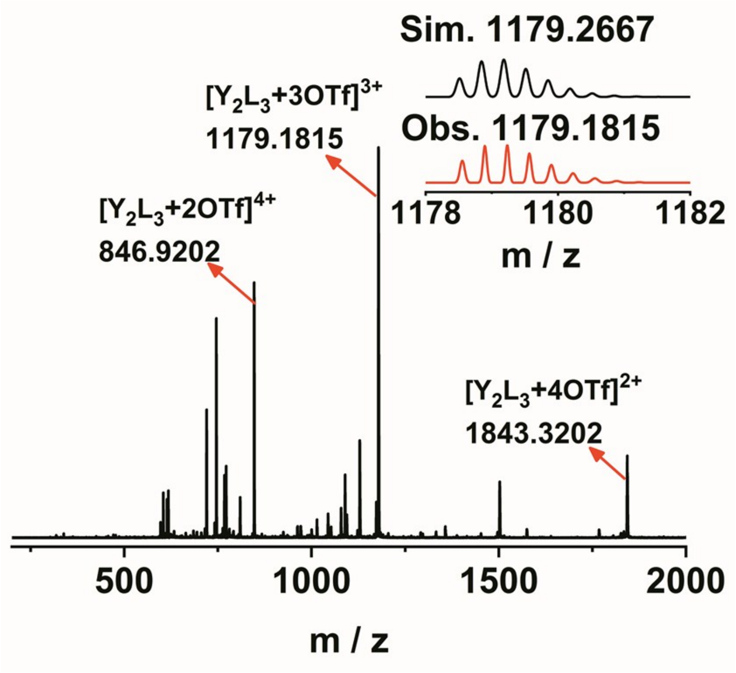

Figure S16. ESI-TOF-MS spectrum of helicate $[\mathrm{Y_2}\,(\mathrm{o}\text{-}\mathbf{L}^{RR})_3](\mathrm{TOf})_6$ with insets showing the observed (Obs.) and simulated (Sim.) isotopic patterns of the anion $[[\mathrm{Y_2}\,(\mathrm{o}\text{-}\mathbf{L}^{RR})_3]\,(\mathrm{TOf})_3]^{3+}$ peaks.

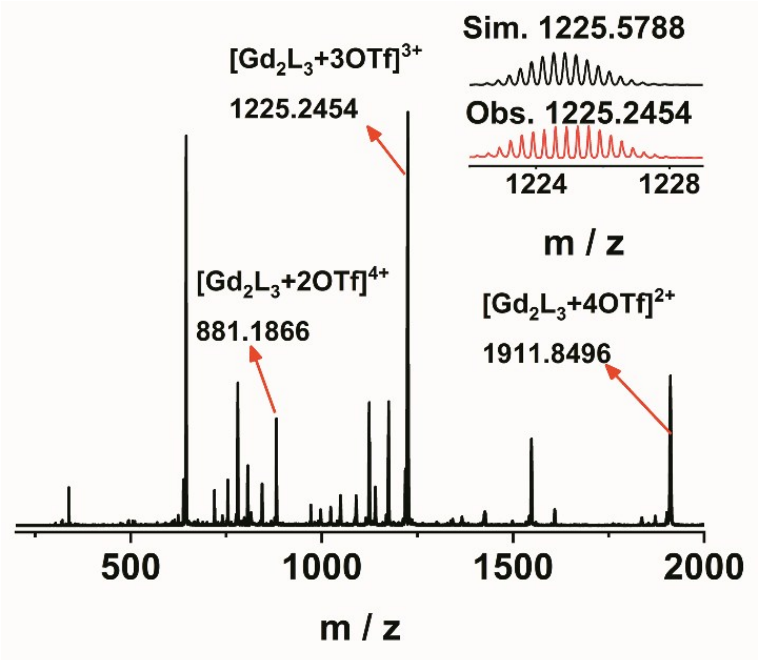

Figure S17. ESI-TOF-MS spectrum of helicate $[Gd_2\,(o\text{-}\mathbf{L}^{SS})_3](TOf)_6$ with insets showing the observed (Obs.) and simulated (Sim.) isotopic patterns of the anion $[[Gd_2\,(o\text{-}\mathbf{L}^{\mathbf{RR}})_3](TOf)_3]^{3+}$ peaks.

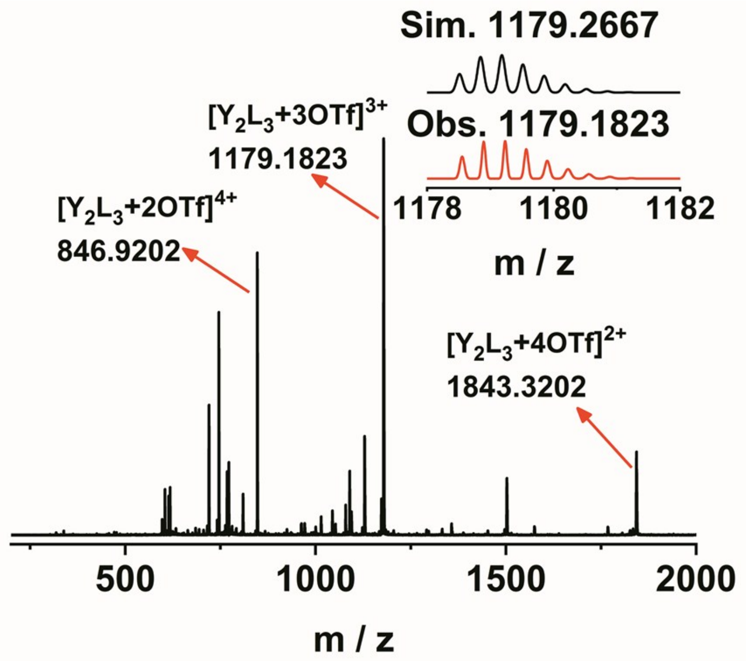

Figure S18. ESI-TOF-MS spectrum of helicate $Y_2\,(o\text{-}\mathbf{L}^{SS})_3(TOf)_6$ with insets showing the observed (Obs.) and simulated (Sim.) isotopic patterns of the anion $[[Y_2\,(o\text{-}\mathbf{L}^{RR})_3](TOf)_3]^{3+}$ peaks.

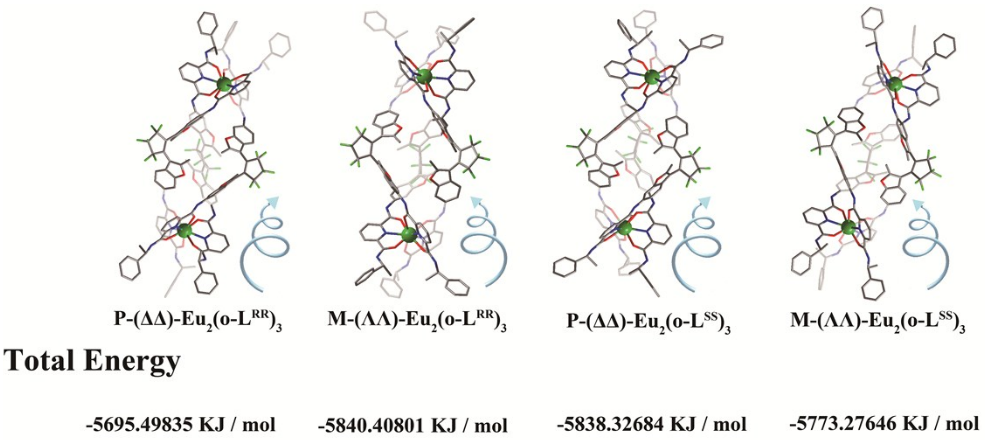

Figure S19. Two possible conformations, *P* or *M* in one helicate based on o-**L**^{RR} and o-**L**^{SS}, and the total energy of each possible helicate. The molecular mechanic modeling was built by using the MOPAC 2016 program implemented in the LUMPAC 3.0 software with a Sparkle/RM1 model.

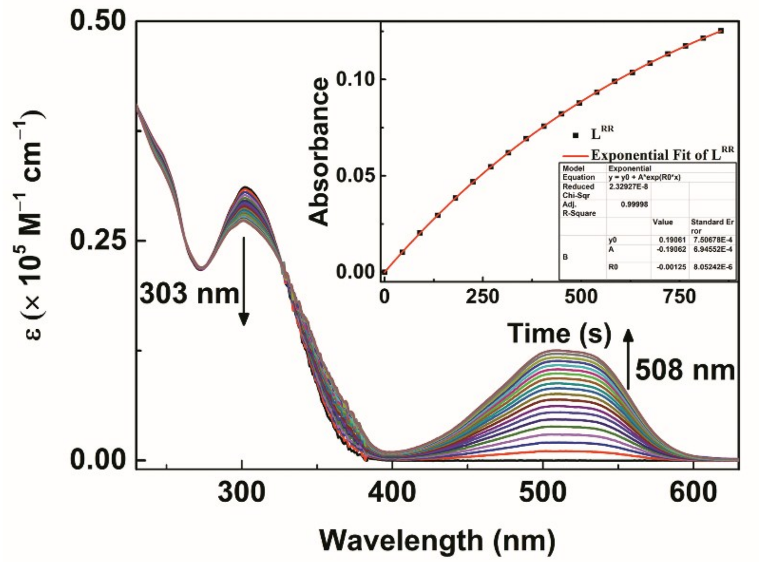

Model	Exponential		
Equation	y = y0 + A*exp(R0*x)		
Reduced Chi-Sqr	2.32927E-8		
Adj. R-Square	0.99998		
		Value	Standard Error
B	y0	0.19061	7.50678E-4
	A	-0.19062	6.94552E-4
	R0	-0.00125	8.05242E-6

Figure S20. UV/Vis spectral changes of o-**L**^{RR} in CH_3CN upon irradiation at 275 nm light (c = 1.0 × 10^{-5} M, $I_{275\ nm}$ = 5.5 × 10^{-5} W/cm^2).

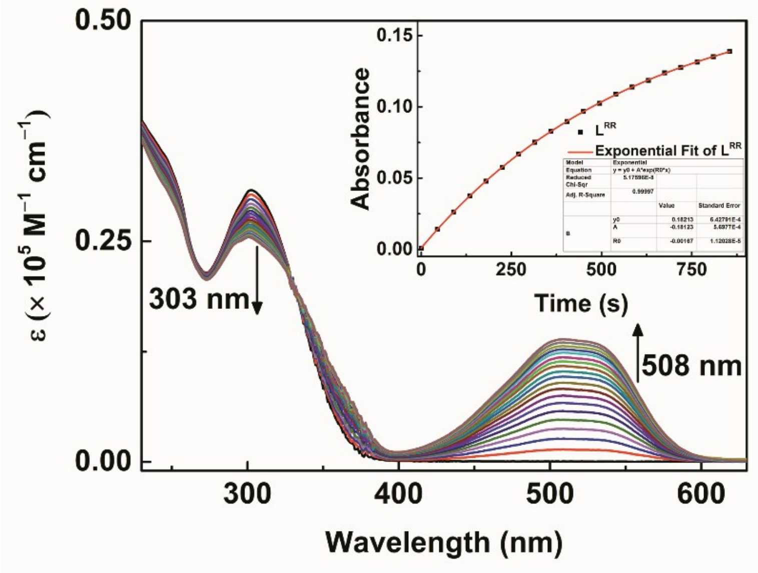

Figure S21. UV/Vis spectral changes of o-**L**^{SS} in CH_3CN upon irradiation at 275 nm light ($c = 1.0 \times 10^{-5}$ M, $I_{275\text{ nm}} = 5.5 \times 10^{-5}$ W/cm^2).

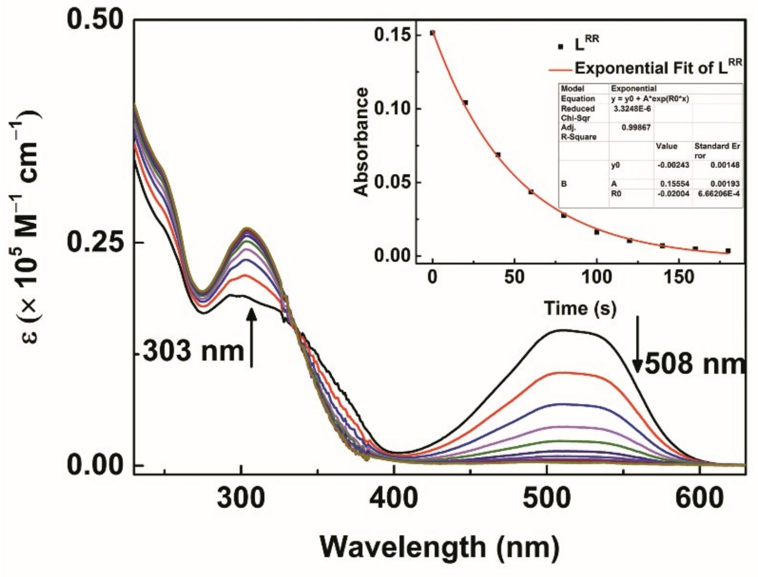

Figure S22. UV/Vis spectra changes of c-**L**^{RR} in CH_3CN upon irradiation at 526 nm light ($c = 1.0 \times 10^{-5}$ M, $I_{526\text{ nm}} = 2.2 \times 10^{-3}$ W/cm^2).

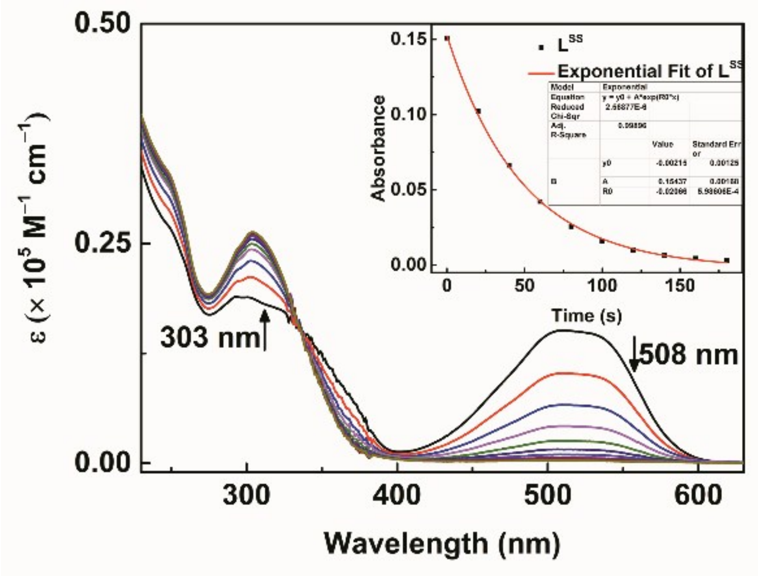

Figure S23. UV/Vis spectra changes of c-$\mathbf{L}^{SS}$ in CH_3CN upon irradiation at 526 nm light (c = 1.0×10^{-5} M, $I_{526\ nm} = 2.2 \times 10^{-3}$ W/cm^2).

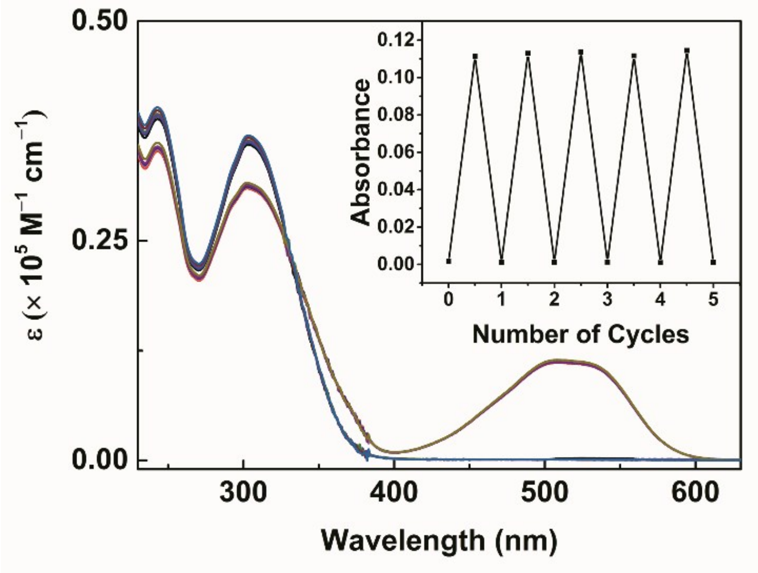

Figure S24. UV/Vis absorbance changes of o-$\mathbf{L}^{RR}$ in CH_3CN on alternate excitation at 275 and 526 nm after five cycles at 293 K. Inset: The absorbance changes at 508 nm upon repeated alternating UV/vis irradiations.

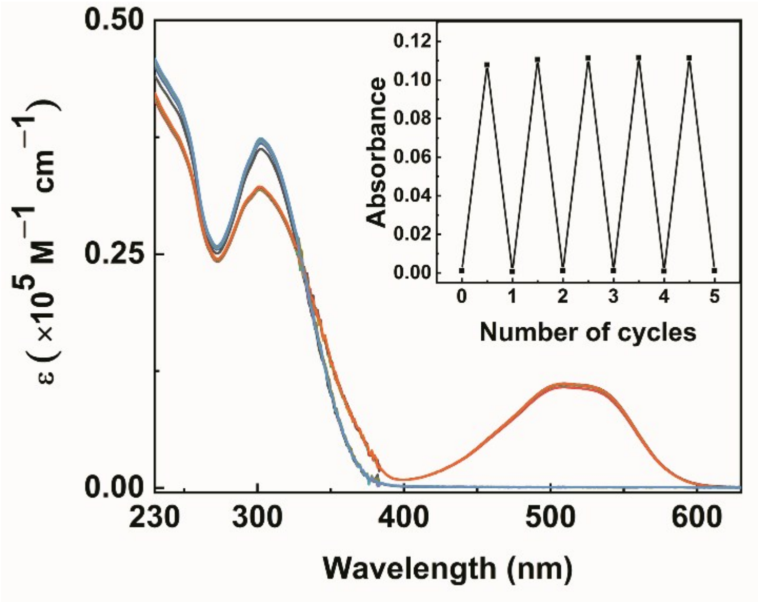

Figure S25. UV/Vis absorbance changes of o-$\mathbf{L}^{SS}$ in CH_3CN on alternate excitation at 275 and 526 nm after five cycles at 293 K. Inset: The absorbance changes at 508 nm upon repeated alternating UV/vis irradiations.

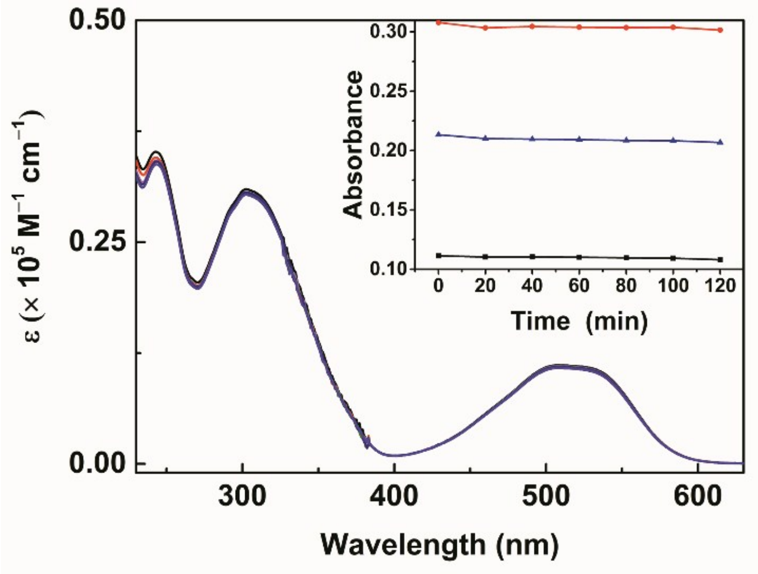

Figure S26. UV/Vis spectra of $\mathbf{L}^{RR}$ in PSS at different heating times (55 °C for 2 h in CH_3CN); no change was observed in shape and intensity, indicating no back reaction to o-**L**. *Insert*: Absorbance changes of the o-**L**/**c-L** mixture monitored at 275, 303, and 508 nm.

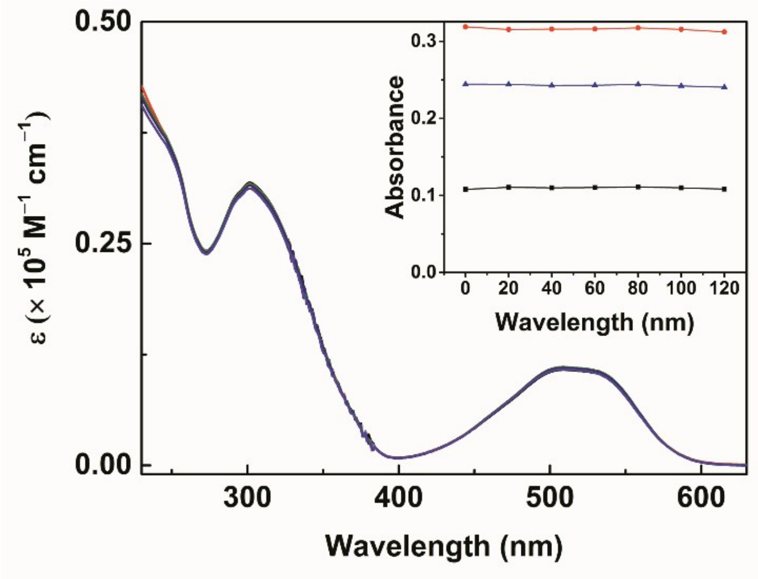

Figure S27. UV/Vis spectra of $\mathbf{L}^{SS}$ in PSS at different heating times (55 °C for 2 h in CH_3CN); no change was observed in shape and intensity, indicating no back reaction to o-**L**. *Insert*: Absorbance changes of the o-**L**/**c**-**L** mixture monitored at 275, 303, and 508 nm.

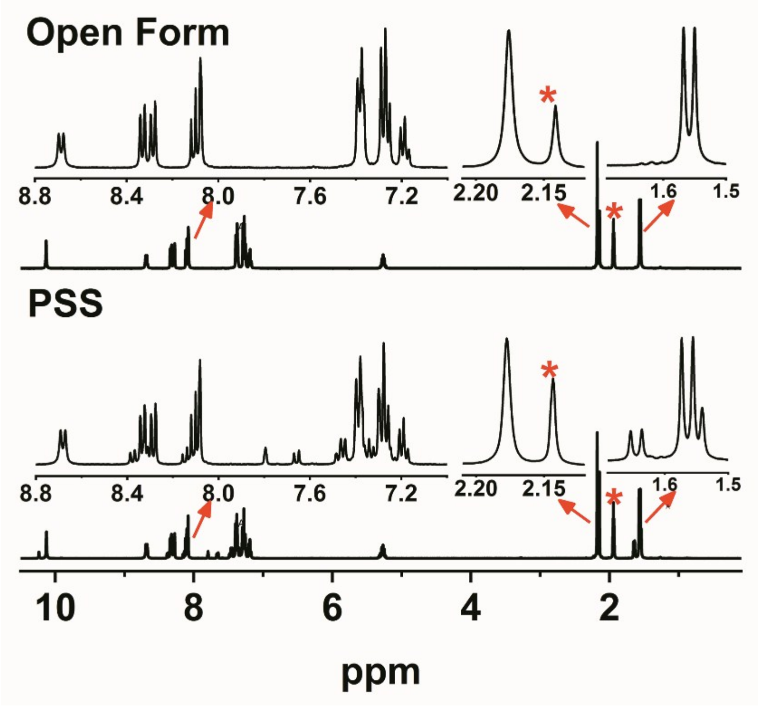

Figure S28. ^{1}H NMR spectra of $\mathbf{L}^{RR}$ in open-ring and PSS states in CD_3CN.

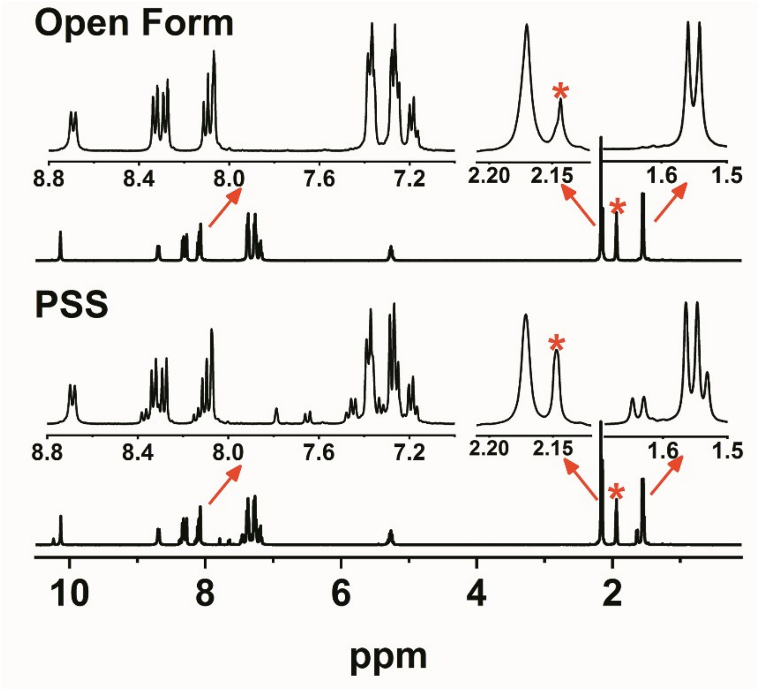

Figure S29. ^{1}H NMR spectra of $\mathbf{L}^{SS}$ in open-ring and PSS states in CD_3CN.

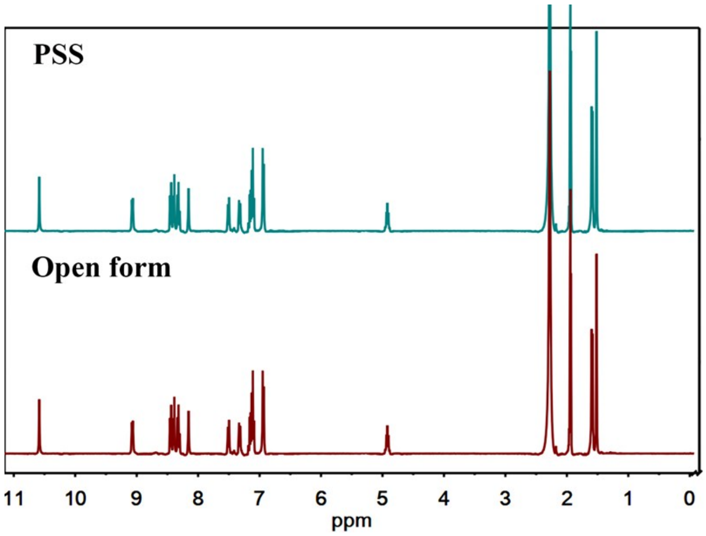

Figure S30. ^{1}H NMR spectra of $[Y_2(\text{o-}\mathbf{L}^{RR})_3](TOf)_6$ (lower curve) and $[Y_2(\mathbf{L}^{RR})_3](TOf)_6$-PSS (upper curve) in CD_3CN.

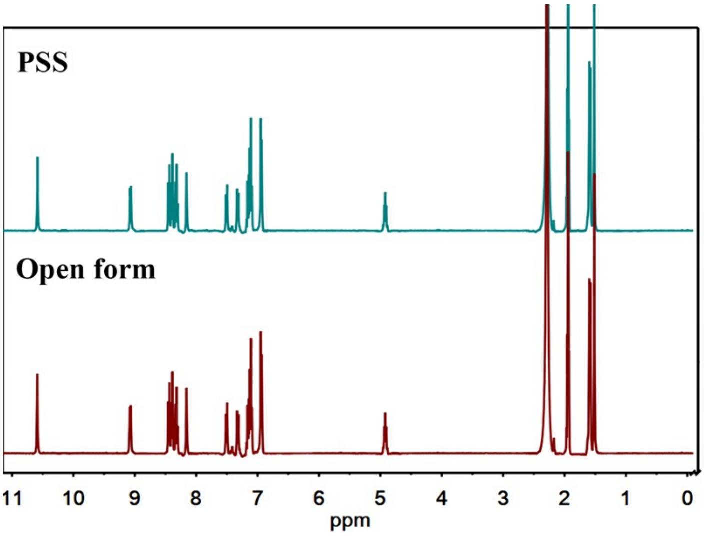

Figure S31. ^{1}H NMR spectra of $[Y_2(\text{o-}\mathbf{L}^{SS})_3](TOf)_6$ (lower curve) and $[Y_2(\mathbf{L}^{SS})_3](TOf)_6$-PSS (upper curve) in CD_3CN.

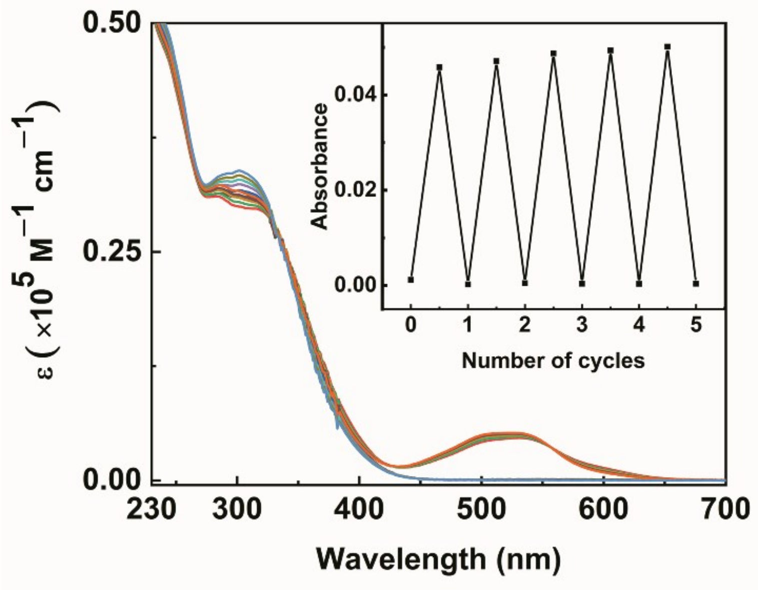

Figure S32. UV/Vis absorbance changes of $[Eu_2(\text{o-}\mathbf{L}^{RR})_3](TOf)_6$ in CH_3CN on alternate excitation at 365 and 526 nm after five cycles at 293 K. Inset: The absorbance changes at 538 nm upon repeated alternating UV/vis irradiations.

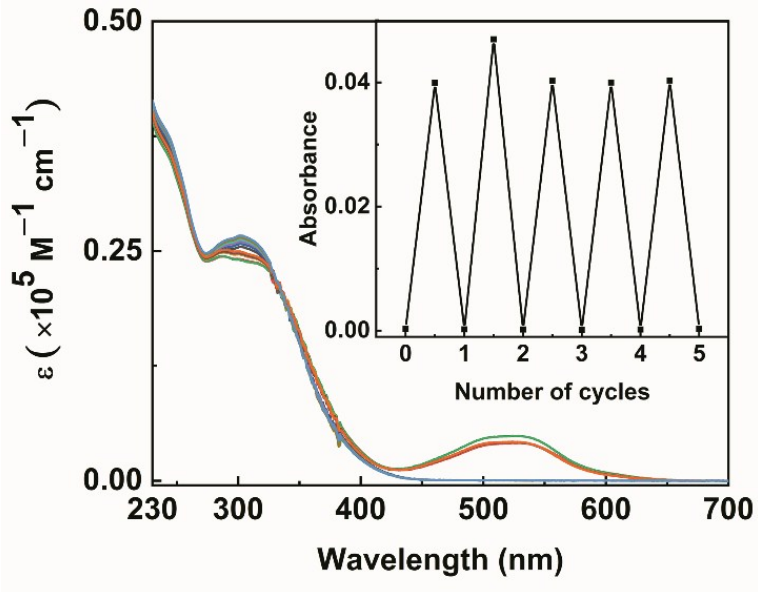

Figure S33. UV/Vis absorbance changes of [Eu_2(o-**L**^{SS})$_3$](TOf)$_6$ in CH_3CN on alternate excitation at 365 and 526 nm after five cycles at 293 K. Inset: The absorbance changes at 538 nm upon repeated alternating UV/vis irradiations.

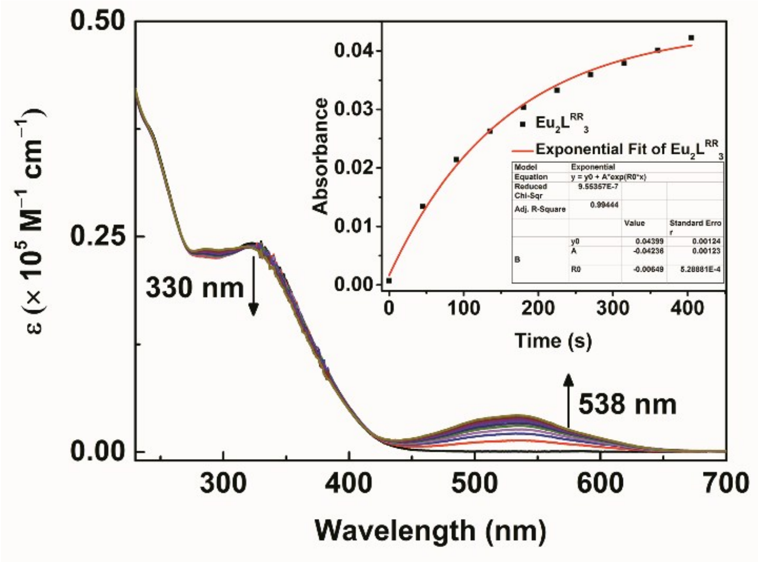

Model	Exponential		
Equation	y = y0 + A*exp(R0*x)		
Reduced Chi-Sqr	9.55357E-7		
Adj. R-Square	0.99444		
		Value	Standard Error
B	y0	0.04399	0.00124
	A	-0.04236	0.00123
	R0	-0.00649	5.28881E-4

Figure S34. UV/Vis spectra changes of [Eu_2(o-**L**^{RR})$_3$](TOf)$_6$ in CH_3CN irradiation at 365 nm light (c = 3.3 × 10^{-6} M, I_{365} = 2.7 × 10^{-3} W/cm^2).

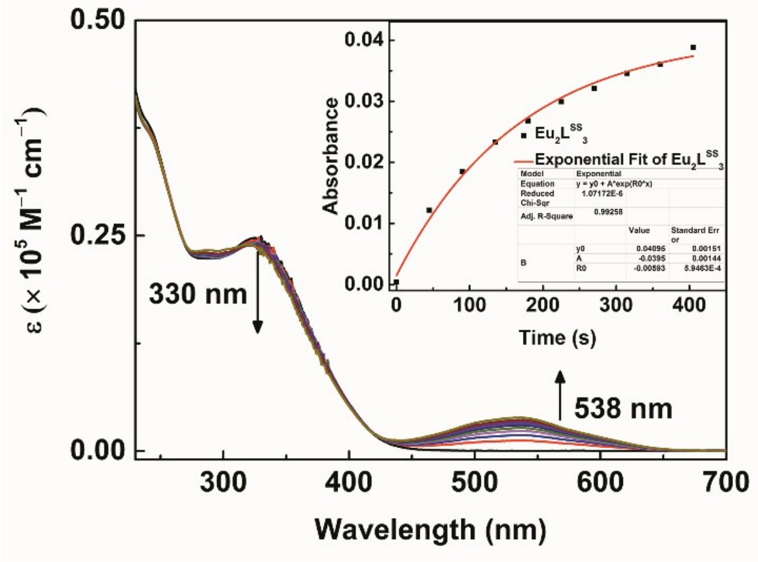

Figure S35. UV/Vis spectra changes of $[Eu_2(o\text{-}\mathbf{L}^{SS})_3](TOf)_6$ in CH_3CN upon irradiation at 365 nm light (c = 3.3 × 10^{-6} M, I_{365} = 2.7 × 10^{-3} W/cm^2).

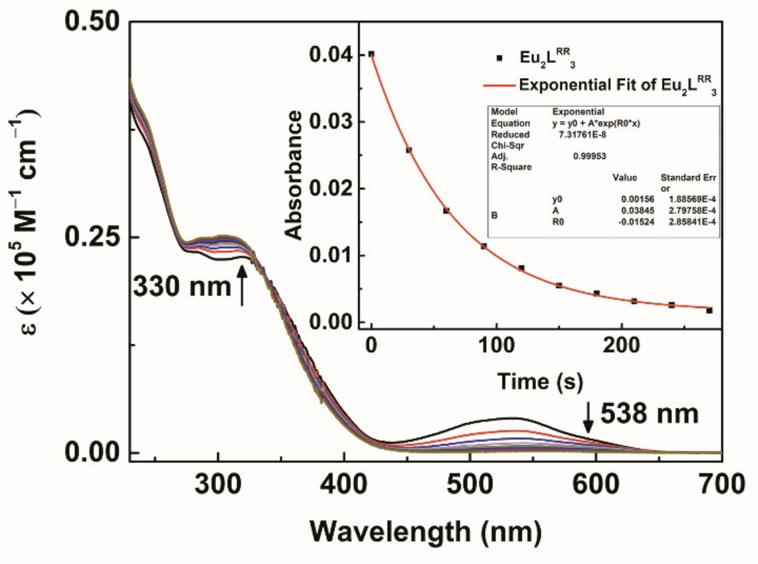

Figure S36. UV/Vis spectra changes of $[Eu_2(\mathbf{L}^{RR})_3](TOf)_6$ in PSS in CH_3CN upon irradiation at 526 nm light (c = 3.3 × 10^{-6} M, $I_{526\ nm}$ = 2.2 × 10^{-3} W/cm^2).

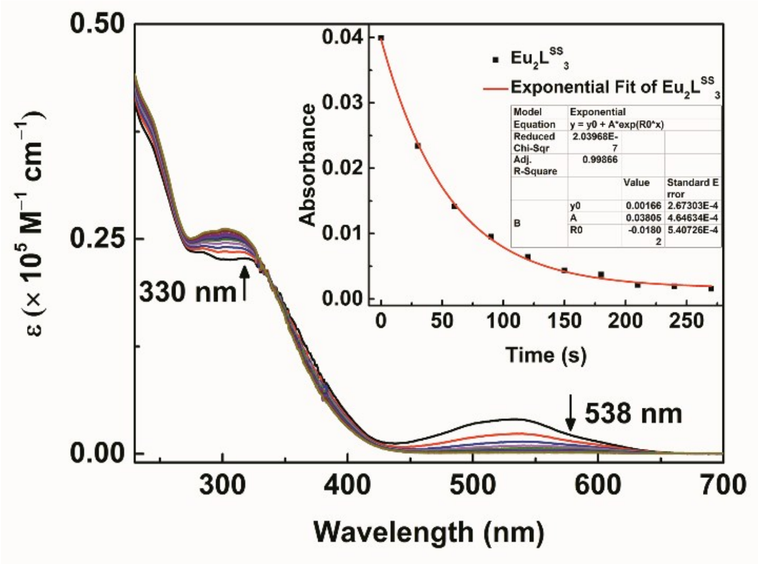

Model	Exponential		
Equation	y = y0 + A*exp(R0*x)		
Reduced Chi-Sqr	2.03968E-7		
Adj. R-Square	0.99866		
		Value	Standard Error
B	y0	0.00166	2.67303E-4
	A	0.03805	4.64634E-4
	R0	-0.01802	5.40726E-4

Figure S37. UV/Vis spectra changes of $[Eu_2(\mathbf{L}^{SS})_3](TOf)_6$ in PSS in CH_3CN upon irradiation at 526 nm light ($c = 3.3 \times 10^{-6}$ M, $I_{526\ nm} = 2.2 \times 10^{-3}$ W/cm^2).

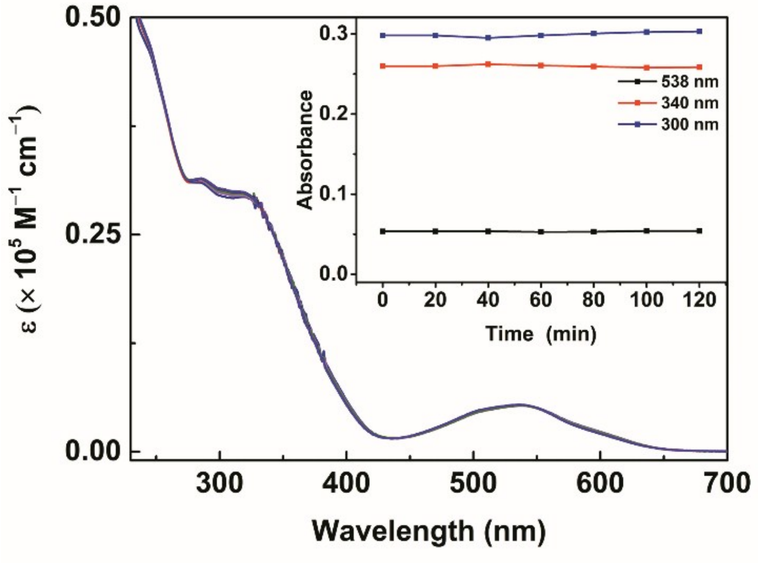

Figure S38. UV/Vis spectra of $[Eu_2(\mathbf{L}^{RR})_3](TOf)_6$ in PSS at different heating times (55 °C for 2 h in CH_3CN); no change was observed in shape and intensity, indicating no back reaction to $[Eu_2(o\text{-}\mathbf{L}^{RR})_3](TOf)_6$. *Insert*: Absorbance changes of the open-ring/close-ring mixture monitored at 300, 340, and 538 nm.

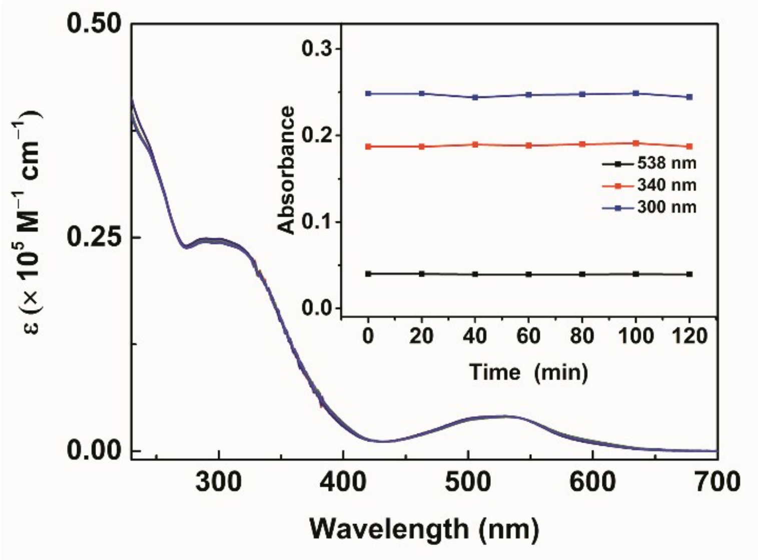

Figure S39. UV/Vis spectra of [$Eu_2(\mathbf{L}^{SS})_3$]($TOf)_6$ in PSS at different heating times (55 °C for 2 h in CH_3CN); no change was observed in shape and intensity, indicating no back reaction to [Eu_2(o-$\mathbf{L}^{SS})_3$]($TOf)_6$. *Insert*: Absorbance changes of the open-ring/close-ring mixture monitored at 300, 340, and 538 nm.

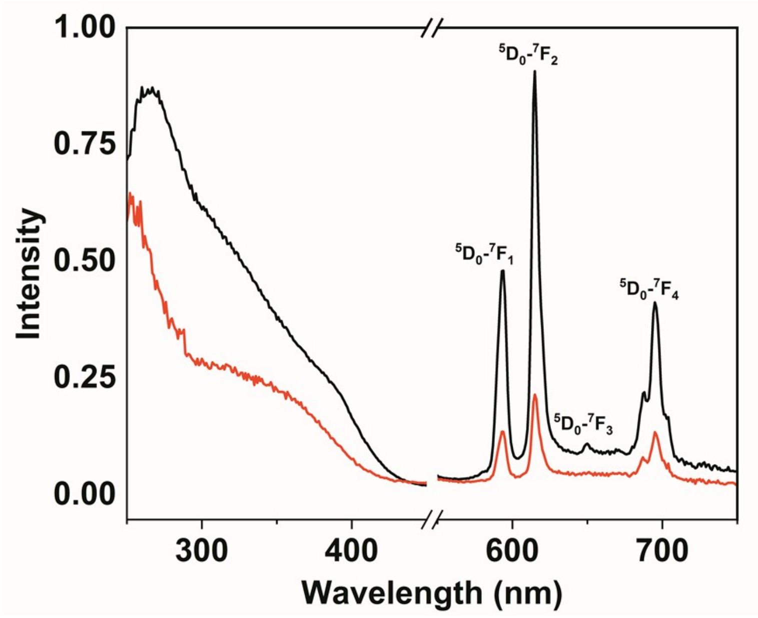

Figure S40. Excitation (left) and emission (right) spectra of [Eu_2(o-$\mathbf{L}^{RR})_3$]($TOf)_6$ (black line) and [Eu_2(**c-**$\mathbf{L}^{RR})_3$]($TOf)_6$ (red line) in CH_3CN (3.3 × 10^{-6} M).

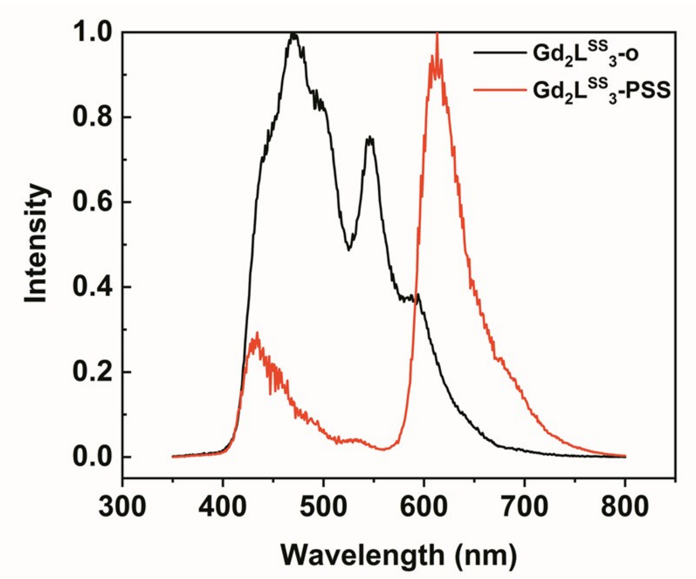

Figure S41. Phosphorescence spectra of [Gd$_2$(o-**L**^{SS})$_3$](TOf)$_6$ (black) and [Gd$_2$(**L**^{SS})$_3$](TOf)$_6$–PSS (red) at 77 K in CH$_3$CN (a delay time of 100 μs was selected to eliminate the possible fluorescence).

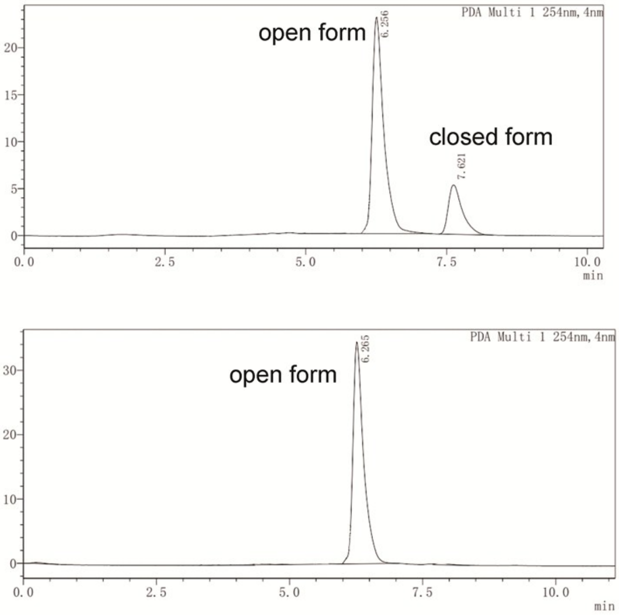

Figure S42. HPLC chromatograms (InertSustain C18 column) of o-**L**^{RR} (lower curve), and **L**^{RR}-PSS (upper curve) eluted with acetonitrile, at a flow rate of 1.0 mL min^{-1}.

Table S1. HPLC analysis of **L**^{RR} in open/close-ring forms.

Peak No.	Ret. Time	Area	Area%
1	6.256	332389	78.7
2	7.621	90652	21.3

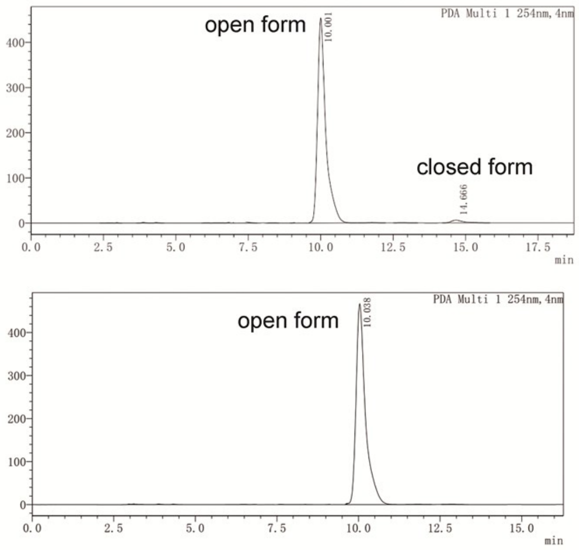

Figure S43. HPLC chromatograms (InertSustain C18 column) of $[Eu_2(o\text{-}\mathbf{L}^{RR})_3](TOf)_6$ (lower curve), and $[Eu_2(\mathbf{L}^{RR})_3](TOf)_6$-PSS (upper curve) eluted with acetonitrile, at a flow rate of 1.0 mL min^{-1}.

Table S2. HPLC analysis of $[Eu_2(o\text{-}\mathbf{L}^{RR})_3](TOf)_6$ in open/close-ring forms.

Peak No.	Ret. Time	Area	Area%
1	10.001	9032262	98.0
2	14.666	179697	2.0

Supplementary Notes

Supplementary Note 1. The cyclization and cycloreversion quantum yields calculation.

The quantum yields of photoisomerization reactions were measured following the reported method (Supplementary Equation 1–7). The kinetics of re-equilibration from an arbitrary initial photostationary state (A_0) to a new phostationary state (A_{pss}) dictated by exposure to light of a given wavelength, is monoexponential (Supplementary Figures S20–S23 and Supplementary Equation 1). The rate constant of equilibration (κ_{eq}) is given by the sum of the two apparent first-order rate constants defining the overall transition and the equilibrium constant (K_{pss}) by their ratio. κ_{ex} is the rate constants for absorption at excitation wavelength. σ_{ex} (cm^2 molecule^{-1}) is the absorption cross-section at excitation wavelength λ_{irr} (nm). ψ_{ex} (photons s^{-1}cm^{-2}) is the photon flux. I (W cm^{-2}) is the intensity of irradiation light, it is 55 μW/cm^2 for 275 nm and 2.2 mW/cm^2 for 526 nm. N_A is the Avogadro's constant. The concentration for $\mathbf{L}^{RR}$ and $\mathbf{L}^{SS}$ in CH_3CN are1.0 × 10^{-5} M.

$$A(t) = A_{pss} + (A_0 - A_{pss})\, e^{-\kappa_{eq} t} \quad (1)$$

$$\kappa_{eq} = \kappa_{o\to c} + \kappa_{c\to o}, \quad (2)$$

$$K_{pss} = [\text{Open form}] / [\text{closed form}] = \kappa_{o\to c} / \kappa_{c\to o} \quad (3)$$

$$a_{pss} = K_{pss} / (1 + K_{pss}) = \kappa_{o\to c} / \kappa_{eq} \quad (4)$$

$$\kappa_{ex} = \sigma_{ex}\, \psi_{ex},\ \sigma_{ex} = (10^3 \ln 10 / N_A)\, \varepsilon_{irr},\ \psi_{ex} = 5 \times 10^{15} \lambda_{irr}\, I \quad (5)$$

$$\Phi_{o\to c} = \kappa_{o\to c} / \kappa_{ex,o} \quad (6)$$

$$\Phi_{c\to o} = \kappa_{c\to o} / \kappa_{ex,c} \quad (7)$$